Solar Energy Materials & Solar Cells 210 (2020) 110481

Contents lists available at ScienceDirect

Solar Energy Materials and Solar Cells

journal homepage: http://www.elsevier.com/locate/solmat

Light-induced-degradation defect independent of the boron concentration: Towards unifying admittance spectroscopy, photoluminescence and photoconductance lifetime spectroscopy results

Fiacre E. Rougieux [a,*], Chang Sun [b], Mattias Juhl [a]

[a] School of Photovoltaic and Renewable Energy Engineering, The University of New South Wales, Sydney, NSW2052, Australia
[b] Research School of Electrical, Energy & Materials Engineering, The Australian National University, Canberra, ACT2601, Australia

ARTICLE INFO

Keywords:
Boron-oxygen defect
Lifetime spectroscopy
Light-induced-degradation
Recombination
Defect
Silicon

ABSTRACT

Recent photoluminescence and admittance spectroscopy measurements point towards the defect responsible for Light-Induced Degradation (LID) being a shallow level. Dopant dependent lifetime spectroscopy and temperature dependent lifetime spectroscopy on the other hand reveal the existence of a deep level driving the recombination activity of the LID defects. There is an apparent disagreement between admittance spectroscopy results and lifetime spectroscopy results. Here we overcome this apparent disagreement and we show that a negative-U defect with one shallow level can explain both the doping dependent lifetime data and injection dependent data. The critical consequence of this model is that it readily explains the dependence of the LID defect on the hole concentration rather than the Boron concentration.

1. Introduction

A specific form of Light Induced Degradation (LID), commonly referred to as a Boron Oxygen defect, has been thoroughly studied for over 40 years [1,2]. Recently the defect responsible for this LID has been directly observed with admittance spectroscopy and photoluminescence spectroscopy. A significant part of the work on LID has been performed with lifetime spectroscopy, a technique that does not provide a direct route to determine the electrical characteristics of defects. This paper attempts to reconcile new admittance spectroscopy results with lifetime spectroscopy measurements.

One of the core results from lifetime spectroscopy, provided by Bothe et al., was that the "effective defect density" of the LID defect was proportional to the boron concentration of the sample [3]. The effective defect density is a measure of the change in recombination, at a fixed excess carrier density. If the defect is located near midgap, the linear trend of the effective defect density with boron concentration suggests the defect concentration is related to the Boron concentration. Similar trends were observed between the effective defect density and the oxygen concentration, and hence the defect became to be known as the boron oxygen defect. However, recent photoluminescence and admittance spectroscopy measurements suggest that the defect responsible for Light-Induced Degradation (LID) is a shallow level at room temperature [4]. As we will show in this paper, a shallow defect level means that the conclusion made based on the results of the lifetime data alone are invalid. We will demonstrate that the proportionality between effective defect density and doping density, can be explained if the actual defect concentration is the same in all samples regardless of doping. Thus, the original interpretation of the linear correlation between the boron oxygen defect and the boron concentration must be reassessed and we must update the model incorporating this new evidence. We however cannot say that the defect does not contain boron, as it does not occur when boron is replaced with gallium.

This paper first reviews the effective defect density as a metric and demonstrates that it is invalid for shallow levels when comparing between samples of different doping. We then present a corrected defect density, an alternative metric that is unaffected by the doping level or injection level if the defect parameters are known. The paper then proposes a new model for the LID defect assuming the LID defect contains a shallow level. We validate the new model against data from doping dependent lifetime spectroscopy, demonstrating improved results particularly for uncompensated material. The paper then reevaluates data from injection level dependent lifetime spectroscopy, modifying the suggested negative-U structure of the LID defect to incorporate a shallow level. Finally, we evaluate critically the new model and look at other apparent contradictions between lifetime

* Corresponding author.
E-mail address: fiacre.rougieux@unsw.edu.au (F.E. Rougieux).

https://doi.org/10.1016/j.solmat.2020.110481
Received 5 August 2019; Received in revised form 20 February 2020; Accepted 22 February 2020
Available online 29 February 2020

spectroscopy and admittance spectroscopy and offer possible explanations for discrepancies.

2. Impact of a shallow level on the effective defect density

As opposed to Deep Level Transient Spectroscopy and admittance spectroscopy, lifetime spectroscopy does not measure the defect density. A proxy for the defect density is to take the inverse of the minority carrier lifetime at a fixed injection level. This is called the effective defect density or normalised defect density and is defined as [5]:

$$N_t^*(t) = \frac{1}{\tau(t)} - \frac{1}{\tau(0)} \tag{1}$$

where τ(t) is the effective lifetime at instant t and τ(0) is the initial effective lifetime.

If only one defect level has been introduced between the two measurements of lifetime, the effective defect density is given by

$$N_t^* = \frac{1}{\tau_{SRH}} \tag{2}$$

Where τ_{SRH} is the Shockley-Read-Hall (SRH) lifetime.

Förster and Herguth, for instance, have recently demonstrated some of the limitations of this metric [6,7]. In this section, we highlight that this definition is only meaningful when performing lifetime measurements on very deep levels.

The relationship between lifetime and the defect density can be found for a monovalent defect from SRH recombination statistics, with the SRH lifetime defined as:

$$\tau_{SRH} = \frac{\tau_{p0}(n_0 + n_1 + \Delta n) + \tau_{n0}(p_0 + p_1 + \Delta n)}{n_0 + p_0 + \Delta n} \tag{3a}$$

where n_0 is the equilibrium electron density, p_0 is the equilibrium hole density and Δn is the excess carrier concentration.

With

$$n_1 = N_C exp\left(\frac{E_C - E_T}{kT}\right) \tag{4a}$$

$$p_1 = N_V exp\left(\frac{E_C - E_G - E_T}{kT}\right) \tag{5a}$$

where E_C-E_T is the defect energy level relative to the conduction band and E_C-E_G-E_T is the defect energy level relative to the valence band.

And

$$\tau_{n0} = \frac{1}{N_t C_n} \tag{6a}$$

$$\tau_{p0} = \frac{1}{N_t C_p} \tag{7a}$$

Where N_t is the defect density, c_n the capture rate for electrons and c_p the capture rate for holes.

The effective defect density is thus:

$$N_t^* = \frac{n_0 + p_0 + \Delta n}{\tau_{p0}(n_0 + n_1 + \Delta n) + \tau_{n0}(p_0 + p_1 + \Delta n)} \tag{8}$$

For p-type silicon, ($n_0 \ll p_0$) with a defect in the lower half of the bandgap ($n_1 \approx 0$) the above expression becomes

$$N_t^* = \frac{p_0 + \Delta n}{\tau_{p0}\Delta n + \tau_{n0}(p_0 + p_1 + \Delta n)} \tag{9}$$

The effective density is evaluated at a constant fraction of the doping to allow comparison between different doping densities, usually $\Delta n = 0.1 \times p_0$:

$$N_t^* = \frac{1.1 \times p_0}{\tau_{p0} 0.1 \times p_0 + \tau_{n0}(p_1 + 1.1 \times p_0)} \tag{10}$$

This is where a crucial assumption is made that the defect being measured is deep enough such that $p_1 \ll p_0$ holds:

$$N_t^* = \frac{1.1 \times p_0}{\tau_{p0} 0.1 \times p_0 + \tau_{n0} 1.1 \times p_0} \tag{11}$$

$$N_t^* = \frac{1}{\frac{\tau_{p0} 0.1}{1.1} + \tau_{n0}}$$

This becomes:

$$N_t^* = \frac{1}{\frac{0.1}{1.1 N C_p} + \frac{1}{N C_e}} \tag{12}$$

$$N_t^* = \frac{N}{\frac{0.1}{1.1 C_p} + \frac{1}{C_n}} \tag{13}$$

The denominator is a constant for different dopant densities and hence:

$$N_t^* \propto N \tag{14}$$

For a sufficiently deep defect the effective defect density is directly proportional to the real defect density, which has been assumed for all the work performed on the LID defect. However, this is not true for defects that have an energy level closer to the band edge than the Fermi energy level. If the LID defect is a shallow ($E_T \simeq E_V + 40$ meV from admittance spectroscopy [4]), it follows that previous lifetime studies making use of the effective defect density to study the boron oxygen defect are inaccurate. To be clear, the assumption a deep defect level of previous literature was based on several experimental indications. As evidence of a shallow level were only reported recently, this assumption was the most sensible at the time.

The doping density required to render the effective defect density inaccurate as a proxy for the defect density occurs for:

$$p_0 > p_1 \tag{15}$$

Substituting Equation (5) provides

$$p_0 > N_V exp\left(\frac{E_C - E_G - E_T}{kT}\right) \tag{16}$$

Resulting in a doping level $p_0 > 7.7 \times 10^{18} cm^{-3}$. That is the effective defect density is not a valid metric for the defect concentration when the number of holes in the dark is less than 7.7×10^{18} cm^{-3}, i.e. for all existing lifetime data on the LID defect. This means that the most effective defect densities measured by lifetime measurements may not be a measure of the defect concentration but an artefact caused by the influence of p_0.

The more appropriate assumption for the level found for admittance spectroscopy is given by $p_1 > p_0$. Placing this restriction in Equation (10) provides

$$N_t^* = \frac{1.1 \times p_0}{\tau_{n0} p_1} \tag{17}$$

$$N_t^* = \frac{1.1 \times p_0 \times N_t}{C_e p_1} \tag{18}$$

When analysing data across a range of dopings, the effective defect density is then proportional to the doping and the defect density:

$$N_t^* \propto p_0 \times N_t \tag{19}$$

Another strategy to measure the effective density would be to apply a correction factor. Here we outline how to obtain such a correction factor. If p_1 and $k = C_e/C_p$ are known, the impact of a shallow level on the effective defect density measured at an injection level of $\Delta n = \gamma\ p_0$ can

be corrected in p-type silicon as follows (for the derivation see Appendix E):

$$N_t^{**} = N_t^* \frac{1+\gamma}{\gamma k + 1 + \gamma + \frac{p_1}{p_0}} \quad (20)$$

As opposed to the effective defect density N_t*, the Corrected Effective Density (CED) N_t** is not affected by n_0, p_0 or Δn. The advantage of such a correction is that it allows for the determination of the effective defect density using the lifetime at any injection and regardless of the sample doping. The disadvantage is that now we require the knowledge of the energy level and capture cross section ratio.

For the common injection level of $\Delta n = 0.1\ p_0$ that is using $\gamma = 0.1$, N_t**:

$$N_t^{**} = N_t^* \frac{1.1}{1.1k + 0.1 + \frac{p_1}{n_0}} \quad (21)$$

Similar expressions are possible to derive for n-type samples, as shown in the appendix.

3. Methodology used for model selection

There are two salient features in recent measurements of the LID defect. The LID defect possesses a shallow level as measured by impedance spectroscopy [4]. Capture through the LID defect also produces hot electrons from defect-Auger capture as measured by photoluminescence measurements [4]. There are a range of recombination statistics beyond Shockley-Read-Hall statistics that capture such phenomena [8]. Because of evidence of a shallow level we use both a monovalent recombination statistics Shockley-Read-Hall and a multivalent recombination statistics Sah-Shockley [9]. Due to evidence of defect-Auger processes we also use a monovalent recombination statistics that take into account defect exciton-enhanced defect-Auger capture Szmytkowski [10–12] and free-carrier defect Auger capture Evans-Landsberg [13] as well as a multivalent recombination statistics taking into account free-carrier defect Auger capture Sah-Shockley-Evans-Landsberg [9,13]. We also use a reduced Sah-Shockley-Evans-Landsberg recombination statistics where hole capture is multiphonon based and electron capture is based on defect-Auger. For a detailed description of the recombination statistics used see Appendix D.

Fig. 1 shows our model selection process. Our fitting procedure consist of a non-linear least squares fitting algorithm based on the Levenberg–Marquardt algorithm [14]. We select the recombination statistics on three grounds: convergence of our specific fitting procedure in obtaining a high quality of fit to the data, no overfitting of the data (simpler is better), requirement of a shallow level and presence of defect Auger capture for electrons.

It was found that for most lifetime spectroscopy data, Shockley-Read-Hall and Szmytkowski statistics were not able to provide a decent quality of fit, thus these statistics are not selected as representative of the LID defect. The full Sah-Shockley-Evans-Landsberg statistics leads to a good fit albeit with 14 parameters; it overfits the dataset. We disregard the full Sah-Shockley-Evans-Landsberg statistics for the LID defect.

A reasonable fit was obtained for Sah-Shockley statistics, Evans-Landsberg statistics and reduced Sah-Shockley-Evans-Landsberg statistics. We believe all the models can equally well represent the data, however the Sah-Shockley based model does not allow for defect Auger capture and the Evans-Landsberg based model does not contain a shallow level. We believe the model that best represent injection dependent lifetime data, dopant dependent lifetime data as well as impedance spectroscopy data (shallow level) and photoluminescence dates (defect-Auger capture) is the Reduced Sah-Shockley-Evans-Landsberg based model. We label this model "RSSEL model" in the rest of the paper.

4. Reanalysis of doping dependent data

The doping dependent lifetime spectroscopy data from first uncompensated silicon and then compensated silicon data is presented and analysed assuming that the defect is a shallow level.

The data in uncompensated silicon is first presented and contrasted against the current Niewelt model [15]. The lifetime data from Bothe et al. is shown in Fig. 2, along with the Niewelt model [15] in a) and two models based on a shallow level in b). Fig. 2a) shows the complex model of the LID defect of Niewelt using two deep levels and requiring that the defect concentration is proportional boron concentration. In Fig. 2b), the same data is presented, however two models are presented that are based on having a shallow defect with a constant defect concentration between the samples. The first model contains a single level defect with a shallow level, and the second model is the final model presented for

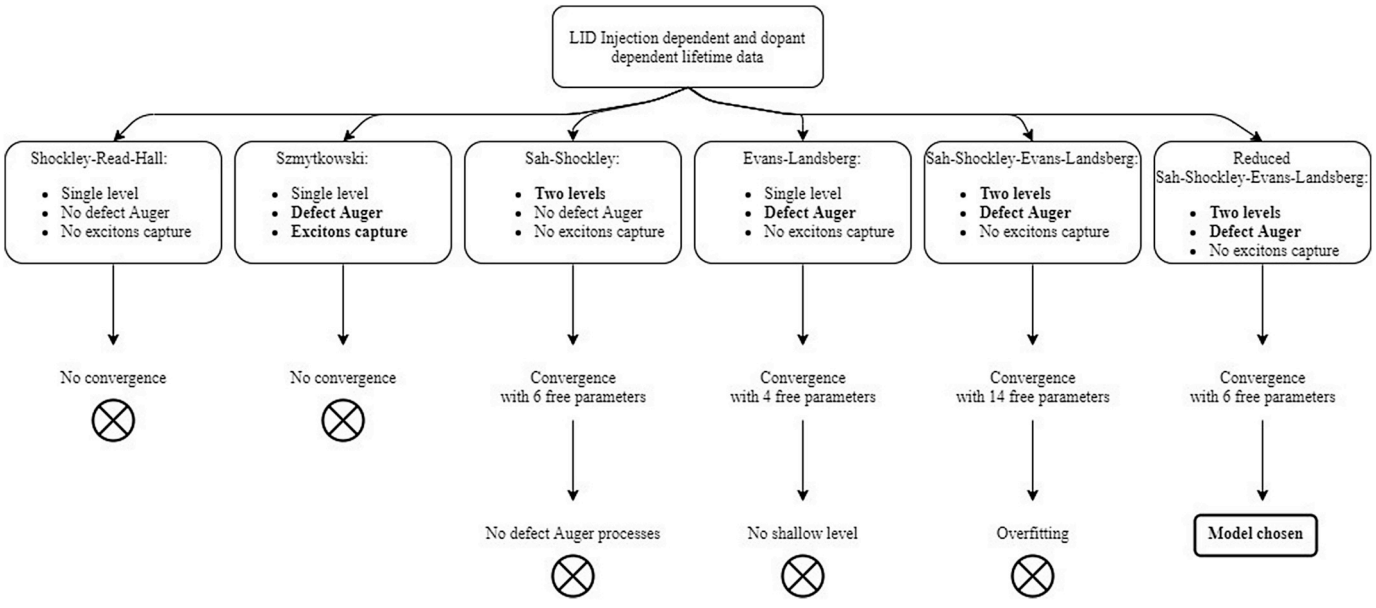

Fig. 1. Model selection methodology. The recombination statistics used are Shockley-Read-Hall, Szmytkowski, Sah-Shockley, Evans-Landsberg, Sah-Shockley-Evans-Landsberg and reduced Sah-Shockley-Evans-Landsberg.

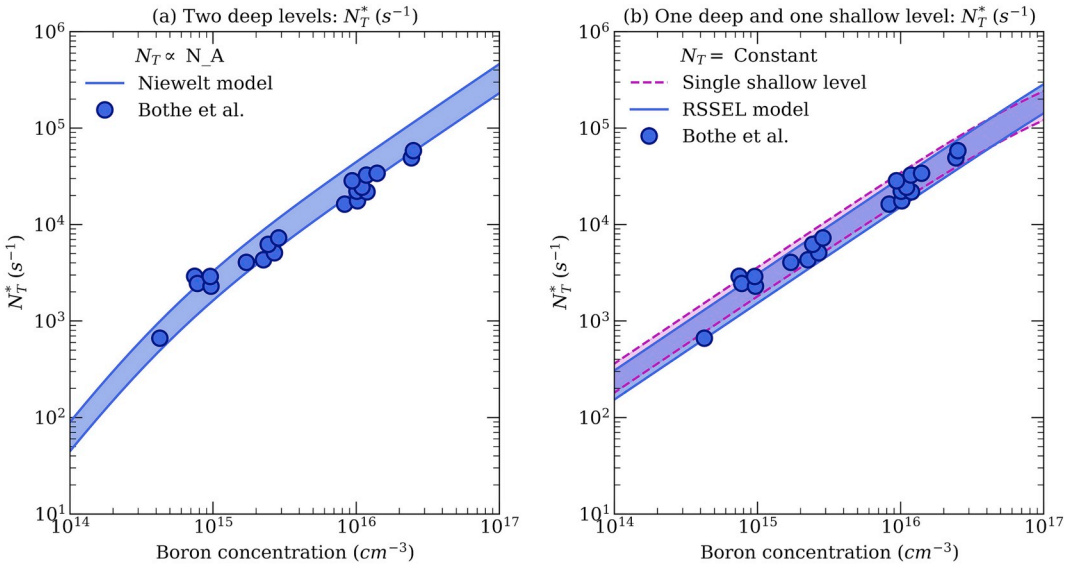

Fig. 2. Comparison of different models that explain that the effective defect density scales with the boron concentration. (a) Niewelt model [15]: Defect density increasing linearly with the net doping and as a result effective defect density increasing with the net doping. (b) RSSEL model: Defect density independent of the net doping. Effective density increasing linearly with the dopant density because of a change of the occupation of the shallow level of the LID defect. The effective defect density data is from Bothe et al.

the LID defect presented later in this paper, to demonstrate that this correctly predicts the injection dependent lifetime results. In both figures the modelling is shown as a wide band. This is used to represent the impact of the variation of interstitial oxygen concentration of the Cz wafers from Bothe et al., being from 7.0×10^{17} to 8.0×10^{17} cm^{-3}. It is observed that all models are able to predict the change in the effective defect density with doping.

One issue with the Niewelt model [15], is that it cannot explain the observed effective defect density in compensated data. In p-type compensated silicon, the defect density scales with the net doping rather than the boron concentration. Several authors modified the Niewelt model to scale with the equilibrium hole concentration rather than the boron concentration. The Niewelt model however cannot easily explain the fact that there is LID in compensated n-type silicon [16,17]. Fig. 3 shows the effective defect density N_t* as a function of the equilibrium hole concentration in compensated p-type and n-type silicon. The data is from Schon et al. [17] and Niewelt et al. [16] as extracted by Schon et al. [17]. The model of Niewelt requires the assumption that the defect density be proportional to the equilibrium hole concentration in p-type silicon and constant in n-type silicon [15–17]. A consequence of the new model proposed here is that it leads to the existence of LID in compensated n-type due to change in the occupation of the defect. Only a model with a shallow level is able to predict the effective defect density in compensated n-type and p-type silicon.

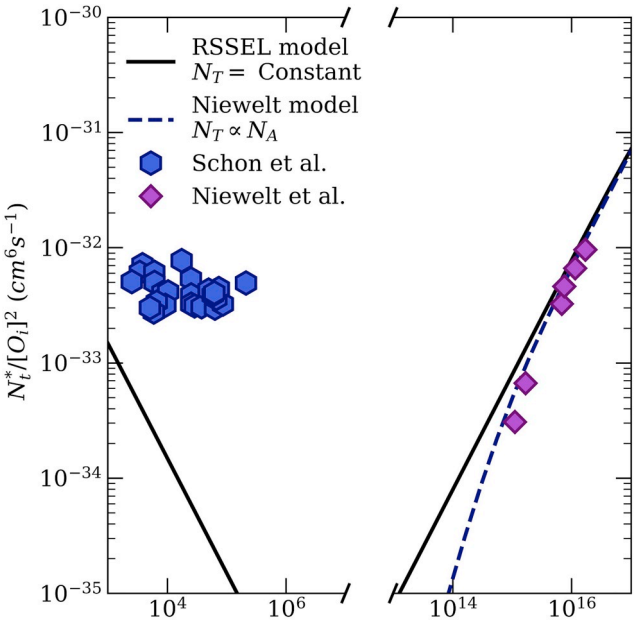

Fig. 3. Effective defect density N_t* as a function of the equilibrium hole concentration in compensated p-type and n-type silicon. The data is from Schon et al. [17] and Niewelt et al. [16] as extracted by Schon et al. [17,17]. The line is a simulation of the effective defect density N_t* for the Niewelt model [15] and the presented model. Only our presented model is in good agreement with experimental data. (For interpretation of the references to colour in this figure legend, the reader is referred to the Web version of this article.)

5. Injection level dependant data

While the doping dependent data is able to predict the lifetime with a single level, it is trivial to demonstrate that a shallow level will not be able to predict the injection dependent lifetime data. However, using a similar model to that of refs [16,18]we will demonstrate that good agreement can be obtained for both injection and doping dependent lifetime.

A review of the previous measured parameters is summarized in Table 1. All the results apart from Vaqueiro-Contreras et al. are based on modelling lifetime data and required more than a single level defect to fit the data. In Table 2., we present three models that accurately describe experimental data without overfitting. These are models using Sah-Shockley recombination statistics, Evans-Landsberg recombination statistics and Reduced-Sah-Shockley-Evans-Landsberg recombination statistics. For the fit obtained using Sah-Shockley statistics and Evans-Landsberg statistics see Appendix B and C. As mentioned in the methodology, though the three models fit the data, we disregard the model based on Evans-Landsberg statistics as it does not contain a shallow level and we disregard the model based on Sah-Shockley recombination statistics as it does not contain defect-Auger capture. We are thus left with the model based on Reduced-Sah-Shockley-Evans-Landsberg recombination statistics. This model has 6 free parameters, and as such may still

Table 1
Parameterisation of the recombination parameters of the LID defect in References [3,4,15,18,24,25].

	Bothe et al. [3]	Schmidt et al. [24]	Rein et al. [25]	Niewelt et al. [15]	Hallam et al. [18]	Vaquero-Contreras et al. [4]
$E_{trap,d}$ (eV)	0.41	E_C - (0.61 ± 0.16)	E_C - 0.410	E_C - (0.34 ± 0.02)	E_C - (0.34 ± 0.01)	single level
$\sigma_{n,d}/\sigma_{p,d}$	10	2.5	9.3	18.1 ± 1	18	single level
$E_{trap,a}$ (eV)	single level	E_V + 0.15	single level	E_V + (0.31 ± 0.02)	E_V + (0.24 ± 0.01)	EV + 0.05
$\sigma_{n,a}/\sigma_{p,a}$	single level	«1	single level	1/(85.7 ± 1.5)	1/(60 ± 6)	not measured
$\sigma_{n,d}/\sigma_{p,a}$	single level	Independent	single level	1.2 ± 0.5	0.2 ± 0.04	single level
N_t (cm^{-3})	$\propto p_0$	$\propto p_0$	$\propto p_0$	$\propto p_0$	$\propto p_0$	not measured

Table 2
Parameterisation of the recombination parameters of the LID defect determined in this work using pure Sah-Shockley statistics (SS), Evans-Landsberg statistics (EL) and Reduced-Sah-Shockley-Evans-Landsberg statistics (RSSEL).

	This paper		
	SS based on Sah-Shockley statistics	EL based on Evans-Landsberg statistics	RSSEL based on Reduced-Sah-Shockley-Evans-Landsberg statistics
See fit in Ref.	Appendix B	Appendix C	This section and appendix A
N_t (cm^{-3})	1×10^{13}	1×10^{13}	1×10^{13}
Level 1			
$E_{trap,d}$ (eV)	EC - 0.10	EC - 0.40	EC - 0.18
$\sigma_{n,d}$ (cm^2)	1.00×10^{-10}	not present	1×10^{-10}
$T_{2,d}$ (cm^2)	no Auger	8.15×10^{-32}	not present
$\sigma_{p,d}$ (cm^2)	4.45×10^{-14}	1.06×10^{-18}	1.8×10^{-15}
$T_{4,d}$ (cm^2)	no Auger	1.38×10^{-33}	not present
Level 2			
$E_{trap,a}$ (eV)	EV + 0.0046	single level	EV + 0.083
$\sigma_{n,a}$ (cm^2)	6.36×10^{-18}	single level	1×10^{-20}
$\sigma_{p,a}$ (cm^2)	1.00×10^{-20}	single level	not present
$T_{3,a}$ (cm^2)	no Auger	not present	1×10^{-10}

have too many degrees of freedom to allow for a precise description of the defect. However, as we will demonstrate, the presented model accurately replicates the LID defects recombination behaviour as a function of net doping and injection level.

The capture cross-sections (1×10^{-10} cm^2 and 1×10^{-20} cm^2) determined are rather extreme values for typical DLTS-measured cross-sections but not unseen. For instance NiH_3 complexes are thought to have capture cross sections for electrons of 2×10^{-11} cm^2 [19] while capture cross sections as high as 3.5×10^{-20} cm^2 have been measured on copper contaminated silicon [20]. The extreme capture cross-section values may point towards further refinement being required for the model.

In addition, note that this model yields a negative-U defect: the donor level is above the acceptor level (the second electron is more strongly bounded than the first) [21]. Sah and Shockley statistics has been used previously to describe recombination at negative-U defects for instance in Ref. [22]. Can Sah and Shockley statistics be not valid for negative-U defect? We believe it is valid if the defect reconfiguration in the intermediate charge state is faster than capture processes. If this condition is met, reconfiguration is not a rate limiting step and does not influence the steady-state defect occupation of the level. This is not the first time that a negative-U structure has been suggested for the LID defect and parametrized using Sah and Shockley statistics (or equivalent). A negative-U structure was first suggested by Voronkov et al. [23] and subsequently

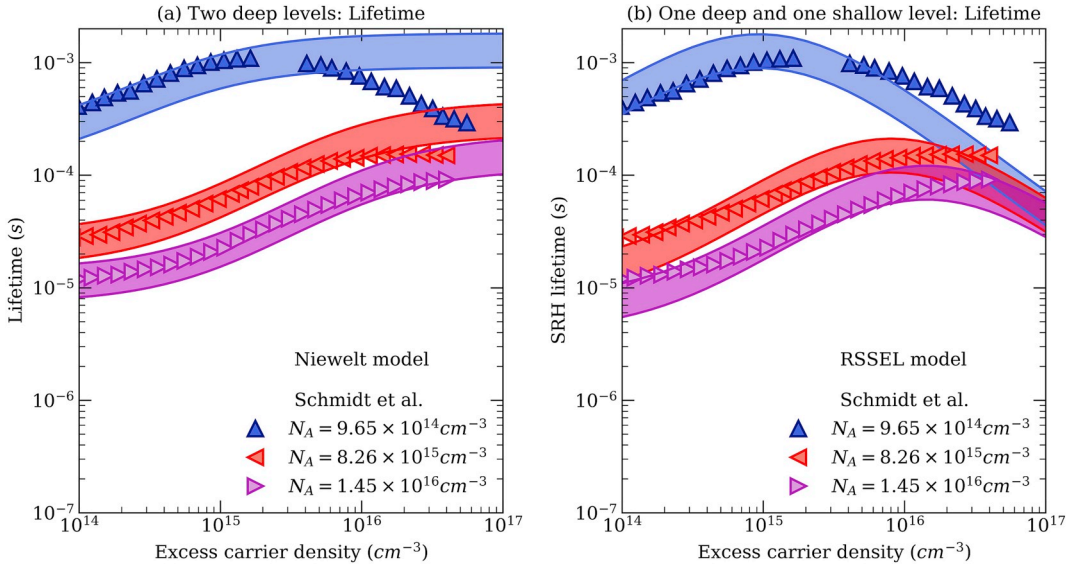

Fig. 4. Comparison of models for the LID defect and its agreement with injection dependent data. (a) Niewelt model [15]: Defect density increasing linearly with the equilibrium hole concentration. As a result, the injection dependent lifetime curves shifts down with increasing net doping. (b) Our model where the defect density independent of the net doping. .

used in injection-dependent lifetime parametrization in and [16–18]. For further details please see the review in Ref. [1].

To demonstrate the ability of the presented model it is now compared to injection dependent lifetime data. Fig. 4 shows the experimental injection dependent lifetime data from Schmidt et al. The Niewelt model [15] and the RSSEL model are presented in Fig. 4a and b for comparison. Again to account for the variation in interstitial oxygen concentration of the Cz wafers from Schmidt et al. (5.5×10^{17} to 7.83×10^{17} cm^{-3}) and modelling is shown as a band. The Niewelt model requires the assumption that the defect density is proportional to the equilibrium hole concentration and as a result, the injection dependent lifetime curve is shifted down for higher dopant densities [15–17]. This is not the case for the presented model, shown in Fig. 4b, which assumes a similar defect concentration in all samples. The low injection lifetime decreases with increasing dopant density because of a change of occupation of the shallow level of the LID defect. While, the high injection data trends to the same lifetime in all samples, as they all have the same electron and hole concentration. Thus, the RSSEL model readily explains the lifetime data without scaling the defect density with the doping density. Fitting over a broader range of dopant densities, injection levels and using data from two independent studies is shown in Appendix A, with a similar good fit being obtained. In the simulation we used a defect density capture cross section product of $N_t\sigma_{n,d} = 1 \times 10^3$ cm^{-1}. Markevich et al. showed that the defect leading to the DLTS signal varies by a factor 10 (5×10^{11} cm^{-3} - 5×10^{12} cm^{-3}) whilst the boron concentration varies by a factor 3.3 (1.4×10^{15} cm-3 – 4.7×10^{15} cm-3 for 3 Ohm–10 Ohm). However, the defect concentration in their study is the defect leading to the DLTS signal, not the recombination active defect but arguably the latent form of the defect. Additionally, the combination of the squared variance in oxygen concentration and linear variance in boron concentration cannot explain the 10-fold variance in defect concentration. Vaqueiro-Contreras did not use a set of varying dopant density to obtain possible dependence of trap concentration on the doping. The recombination active defect concentration as measured by Impedance Spectroscopy in their study is one order of magnitude higher 1×10^{13} cm^{-3}. We choose this defect concentration as a working hypothesis for our model.

5.1. *Effective defect density, a measure of the occupation fraction of the negative-U defect*

One way to understand the dependence of the effective density on the doping is to look at the occupation fraction of the negative-U defect as a function of doping. Through our modelling, we observe that the recombination activity of the LID defect scales with the fraction of defects in a neutral charge state. Fig. 5 shows the fraction of LID defects in neutral charge state as a function of the hole concentration assuming an excess carrier density equal to 10% of the net doping. The further away from midgap, the greater the concentration of LID defect in neutral charge state. As a result, the greater the boron concentration, the higher the effective defect density. As we will see below, this trend also extends to compensated n-type silicon.

6. Discussion

There appears to be two possible interpretations of the increase of the effective defect density with net doping. Interpretation 1, Niewelt model [3,15]: the defect density increases linearly with the net doping, so does the effective defect density. Interpretation 2: the effective defect density is not proportional to the defect density. The first interpretation is the commonly accepted explanation; however, it is hard to reconcile with a defect level close to the band edge such as for the LID defect. The second interpretation allows to both use a shallow level and explain the doping dependence of the LID defect with one less free parameter.

One obvious piece of evidence against interpretation 1 (Niewelt model) is the fact that it requires an additional free parameter, namely

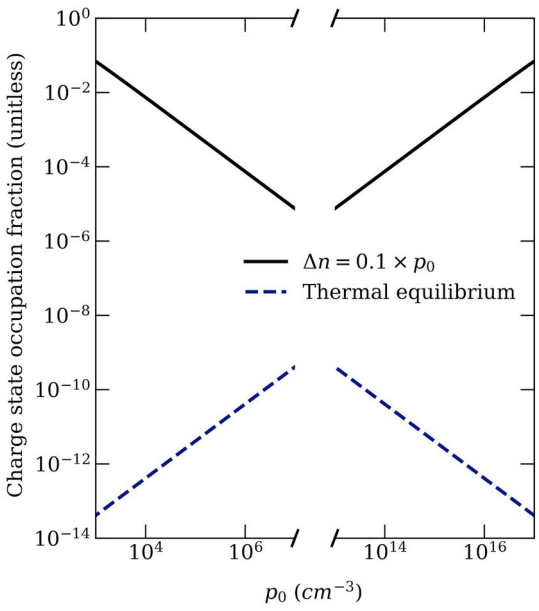

Fig. 5. Fraction of neutral LID defect as a function of the hole concentration. The first simulation (bottom curve) shows the occupation assuming thermal equilibrium. In this case, the neutral occupation fraction is higher when the Fermi level is midgap as expected for a negative-U defect. The second simulation (top curve) shows the occupation assuming an excess carrier density equal to 10% of the net doping. The neutral occupation fraction is now higher when the Fermi level is closer to band edges. In p-type silicon, this leads the fraction of neutral LID defect to increase linearly with the net doping, leading to a linear increase of the effective defect density. (For interpretation of the references to colour in this figure legend, the reader is referred to the Web version of this article.)

that the LID defect concentration scales with the net doping. This assumption is meant to arise from the LID defect requiring a boron atom. However, for other defects where boron is involved e.g. FeB and CrB, this trend is not found, as there is orders of magnitude more boron than the latent defect. Thus, we suggest it is the more robust, and intuitive assumption that the defect is independent of the boron concentration. In addition, a complex model is needed in the Niewelt model [15] to explain the dependence of the effective defect density in p-type silicon (linear dependence) and n-type silicon (constant). In contrast, this complex dependence is a natural consequence of interpretation 2 presented in this paper.

One evidence against our presented model is the temperature dependent lifetime data from Rein et al. [25]. This data suggests that a deep level rather than a shallow level limits the lifetime of p-type silicon wafers. This is because the low-injection lifetime increased only at high temperatures in their measurements. The author assumed that the emission rate became larger than the equilibrium hole concentration at high temperatures meaning the defect must be closer to midgap than the band edge. This is a reasonable assumption; an alternative explanation would be that the lifetime increase at high temperatures is not caused by an increase in carrier emission from a deep defect but due to reduced defect concentration as a result of defect deactivation. Further evidence to this, Rein et al. noted that the lifetime of their sample was limited by a defect with an energy level of ~50 meV from the band edge, as the temperature was reduced, however little attention has been given to this result. Additionally, the fitting of temperature dependent lifetime measurements requires an additional four assumptions for the temperature dependence of the four capture cross sections (two levels). Fitting the data of Rein et al. is a worthwhile exercise but beyond the point of this paper.

Another objection for the proposed model is the absence of a level close to the conduction band detected by DLTS or MCTS. DLTS

measurements were done on p-type silicon wafers. As the level reside in the upper half of the bandgap, DLTS measurements on p-type silicon cannot detect the proposed level. MCTS measurements were also conducted on p-type wafers. The minority capture cross section is significantly smaller than the electron capture for the deep level which would make challenging for the level close to the conduction band to be detected by MCTS.

Finally, both a model incorporating Auger-processes (Evans-Landsberg recombination statistics) and no Auger processes (Sah-Shockley statistics) explains the experimental data [9,13]. The reasonable fit obtained with pure Sah-Shockley may be interpreted as defect-Auger not being a significant capture mechanism, and that multiphonon or cascade-capture processes are acting in parallel, however we have no way to confirm this for the LID defect with the data currently available. There is evidence that multiple capture mechanisms can act in parallel in other absorbers, for instance, the B centre in GaAs shows defect Auger capture in parallel to multiphonon capture [26]. For the B centre, Auger capture dominates at low temperatures and multiphon capture dominates at high temperatures [26]. It is possible that a similar mechanism occurs for the LID defect and further measurements are required to validate this hypothesis.

7. Conclusions

Previous models of the LID defect [16,18] assume a negative-U defect with two deep levels but requires an additional free parameter, namely that the LID defect concentration scales with the net doping. Here we introduce a new model for the LID defect that does not require the LID defect concentration to scale with the net doping but only with the oxygen concentration. As in the Niewelt model, the new model assumes that the recombination active LID defect is a negative-U defect. As opposed to the Niewelt model (and in agreement with recent impedance spectroscopy measurements and low temperature photoluminescence measurements), the new model assumes that the LID defect contains one shallow level. Additionally, electron capture at the shallow acceptor level occurs through a defect-Auger process.

A natural consequence of our new model is that the occupation fraction of the negative-U defect is modulated by the hole concentration. Thus, even though the defect concentration is constant for different boron concentrations, the effective defect concentration as measured by lifetime measurements increases linearly with the doping (at $\Delta n = 0.1 \times p_0$). This hypothesis brings greater consistency between admittance spectroscopy measurements, photoluminescence spectroscopy measurements, infection dependent lifetime spectroscopy measurements and doping dependent lifetime spectroscopy measurements although some questions remain unanswered.

The new model brings accurate and quantitative descriptions of dopant and injection dependent lifetime data in p-type silicon (including compensated p-type silicon). A proper description of n-type data is necessary for a physically correct model but was beyond the scope of this work. The agreement with dopant dependent data in n-type silicon remains qualitative and further work is required to refine the model in n-type silicon.

Finally, we outline a new procedure to fit dopant and injection-dependent lifetime spectroscopy whereby the recombination statistics is not assumed to be Shockley-Read-Hall but all reasonable recombination statistics are used (Shockley-Read-Hall, Szmytkowski, Sah-Shockley, Evans-Landsberg and combinations) and the simpler one in agreement with all datasets is selected.

Author contributions section

F.R. conceived the idea and conducted the modelling. M. J. contributed to the modelling and discussions, C.S. contributed to the modelling and discussions. All authors reviewed the manuscript.

Declaration of competing interest

The authors declare that they have no known competing financial interests or personal relationships that could have appeared to influence the work reported in this paper.

Acknowledgements

This work was supported by the Australian Research Council (ARC) Discovery Early Career Researcher Award (DECRA) project DE160101368 and ACAP project 1-SRI001.

Appendix

Appendix A. Additional injection dependent lifetime data fit for the RSSEL model

The interstitial oxygen concentration of the Cz wafers from Schmidt et al. varies from 5.5×10^{17} to 7.83×10^{17} cm^{-3} and from Niewelt et al. varies from 5.0×10^{17} to 7.0×10^{17} cm^{-3} and thus the fit is made as a fitting band to take into account the variation in the oxygen concentration between different samples. Figure 6 shows the experimental injection dependent lifetime data from Schmidt et al. and Niewelt et al. together with the fit using the Niewelt model and the RSSEL model with parameters from Table 2.

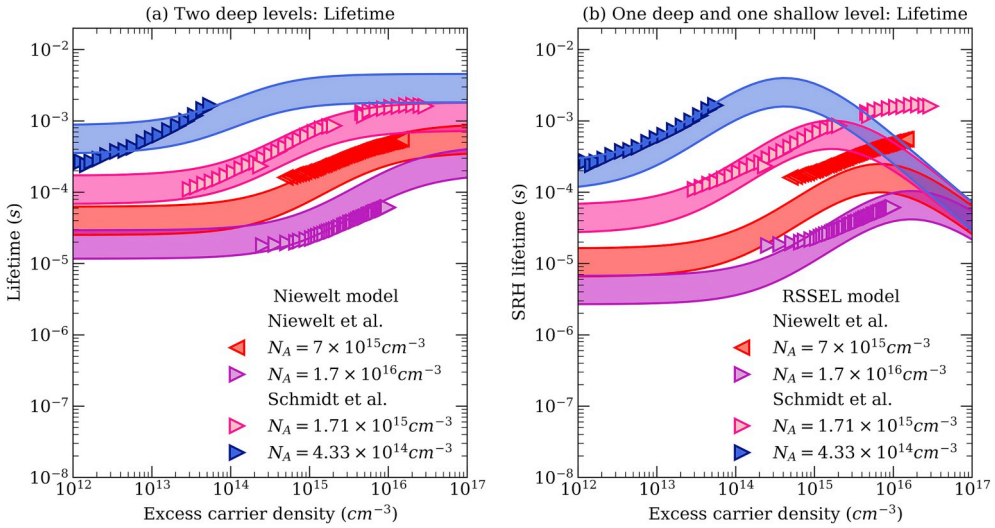

Fig. 6. (a) Niewelt model: Defect density increasing linearly with the net doping. As a result, the injection dependent lifetime curves shifts down with increasing net doping. (b) RSSEL model: Defect density independent of the net doping. The low injection lifetime decreases with increasing dopant density due to a change of occupation of the shallow level of the LID defect. The high injection data leads to similar lifetime in all samples. The injection dependent data is from Schmidt et al. [3]and Niewelt et al. [16].

Appendix B. Sah-Shockley statistics without defect-Auger

Figure 7 shows the experimental injection dependent lifetime data from Bothe et al., Schmidt et al., Niewelt et al. and Schon et al. together with our fit using a multivalent defect using Sah-Shockley recombination statistics with parameters from Table 2.

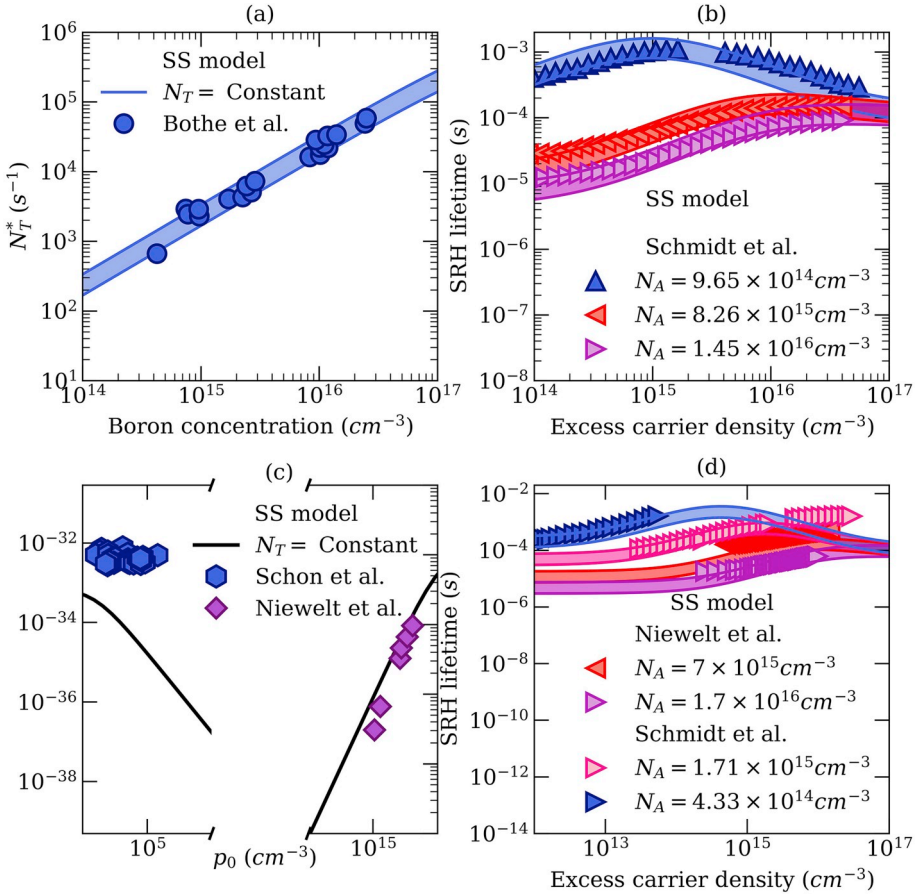

Fig. 7. Defect density independent of the net doping and multivalent defect with a shallow level: (a) Effective density increasing linearly with the dopant density because of an increased capture at high injection due to a change in the occupation fraction of the defect with change in the fermi level. The effective defect density data is from Bothe et al. (b) and (c) Injection dependent lifetime. The low injection lifetime decreases with increasing dopant density due to a change in the occupation fraction of the defect with the quasi-Fermi levels. The injection dependent data is from Schmidt et al. [3] and Niewelt et al. [16]. (d) Effective defect density N_t^* as a function of the equilibrium hole concentration in compensated p-type and n-type silicon. The data is from Schon et al. and Niewelt et al.

Appendix C. Evans and Landsberg statistics using single level

Figure 8 shows the experimental injection dependent lifetime data from Bothe et al., Schmidt et al., Niewelt et al. and Schon et al. together with our fit using a single level operating with Evans-Landsberg recombination statistics with parameters from Table 2.

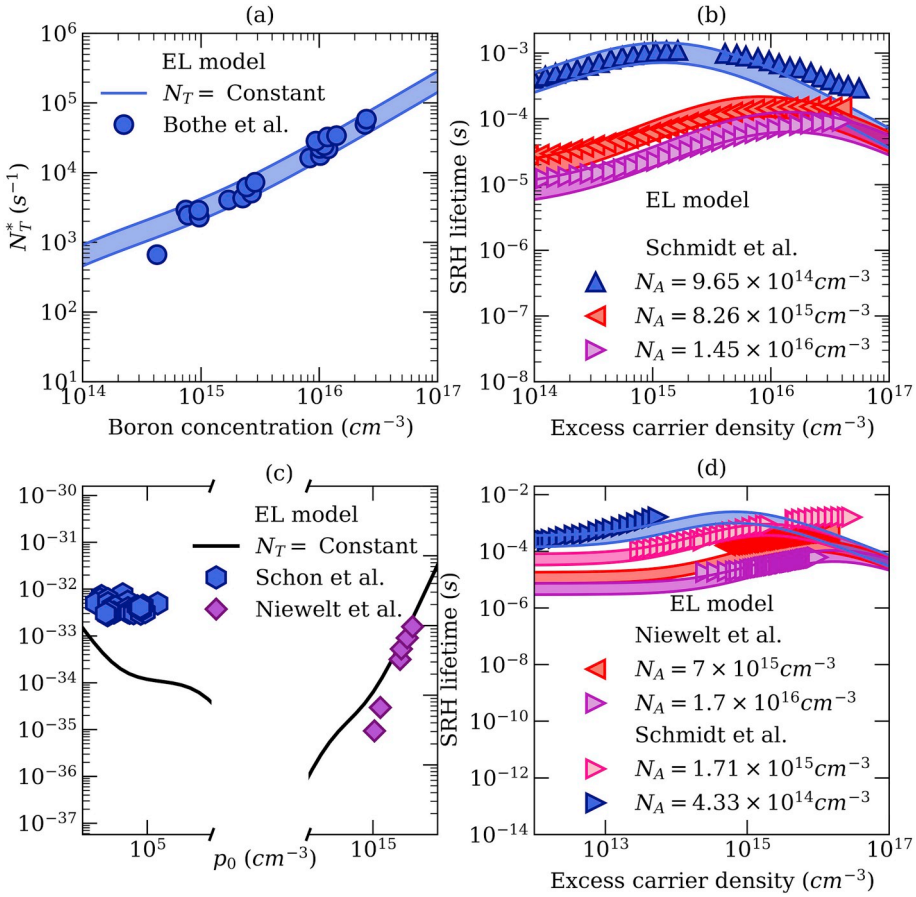

Fig. 8. Defect density independent of the net doping and single level operating with defect Auger processes: (a) Effective density increasing linearly with the dopant density because of an increased capture at high injection due to hole-related defect-Auger capture processes. The effective defect density data is from Bothe et al. (b) and (c) Injection dependent lifetime. The low injection lifetime decreases with increasing dopant density due to increase hole-related defect-Auger capture processes. The injection dependent data is from Schmidt et al. [3] and Niewelt et al. [16]. (d) Effective defect density N_t* as a function of the equilibrium hole concentration in compensated p-type and n-type silicon. The data is from Schon et al. and Niewelt et al.

Appendix D. Description of the recombination statistics used in this paper

Shockley-Read-Hall Statistics:
This statistics is derived in Refs. [27,28]:

$$\tau_{SRH} = \frac{\tau_{p0,SRH}(n_0 + n_1 + \Delta n) + \tau_{n0,SRH}(p_0 + p_1 + \Delta n)}{n_0 + p_0 + \Delta n} \tag{3b}$$

where n_0 is the equilibrium electron density, p_0 is the equilibrium hole density and Δn is the excess carrier concentration.
With

$$n_1 = N_C exp\left(\frac{E_C - E_T}{kT}\right) \tag{4b}$$

$$p_1 = N_V exp\left(\frac{E_C - E_G - E_T}{kT}\right) \tag{5b}$$

And

$$\tau_{n0,SRH} = \frac{1}{N_t \sigma_n v_{th}} \tag{6b}$$

$$\tau_{p0,SRH} = \frac{1}{N_t \sigma_p v_{th}} \tag{7b}$$

Evans-Landsberg Statistics:

This statistics is derived in Ref. [13]:

$$\tau_{EL} = \frac{\tau_{p0,EL}(n_0 + n_1 + \Delta n) + \tau_{n0,EL}(p_0 + p_1 + \Delta n)}{n_0 + p_0 + \Delta n} \tag{3c}$$

where n_0 is the equilibrium electron density, p_0 is the equilibrium hole density and Δn is the excess carrier concentration.

With

$$n_1 = N_C exp\left(\frac{E_C - E_T}{kT}\right) \tag{4c}$$

$$p_1 = N_V exp\left(\frac{E_C - E_G - E_T}{kT}\right) \tag{5c}$$

And

$$\tau_{n0,EL} = \frac{1}{N_t(\sigma_n + T_1 \times n + T_2 \times p)v_{th}} \tag{6c}$$

$$\tau_{p0,EL} = \frac{1}{N_t\left(\sigma_p + T_3 \times n + T_4 \times p\right)v_{th}v_{th}} \tag{7c}$$

Sah-Shockley Statistics:

This statistics is derived in Ref. [9]:

$$\tau_{SS} = \frac{1}{\frac{1}{\tau_1} + \frac{1}{\tau_2}} \tag{22a}$$

With

$$\tau_1 = \frac{\tau_{p0,1}(n_0 + n_{1,1} + \Delta n) + \tau_{n0,1}\left(p_0 + p_{1,1} + \Delta n\right)}{n_0 + p_0 + \Delta n} \tag{23a}$$

$$\tau_2 = \frac{\tau_{p0,2}(n_0 + n_{1,2} + \Delta n) + \tau_{n0,2}\left(p_0 + p_{1,2} + \Delta n\right)}{n_0 + p_0 + \Delta n} \tag{24a}$$

where n_0 is the equilibrium electron density, p_0 is the equilibrium hole density and Δn is the excess carrier concentration.

And

$$\tau_{n0,1} = \frac{1}{N_2\sigma_{n,1}v_{th}} \tag{25a}$$

$$\tau_{p0,1} = \frac{1}{N_2\sigma_{p,1}v_{th}} \tag{26a}$$

$$\tau_{n0,2} = \frac{1}{N_2\sigma_{n,2}v_{th}} \tag{27a}$$

$$\tau_{p0,2} = \frac{1}{N_2\sigma_{p,2}v_{th}} \tag{28a}$$

And

$$N_1 = N_s + N_{s+1} \tag{29a}$$

$$N_2 = N_{s+1} + N_{s+2} \tag{30a}$$

And

$$N_{s+1} = \frac{N_t}{\alpha_1 + 1 + \frac{1}{\alpha_2}} \tag{31a}$$

$$N_s = \alpha_1 N_{s+1} \tag{32a}$$

$$N_{s+2} = \frac{N_{s+1}}{\alpha_2} \tag{33}$$

And

$$\alpha_1 = \frac{k_1 + n_{1,1} + p}{k_1 \times n + p_{1,1}} \tag{34}$$

$$\alpha_2 = \frac{k_2 + n_{1,2} + p}{k_2 \times n + p_{1,2}} \tag{35}$$

And

$$k_1 = \frac{\sigma_{n,1}}{\sigma_{p,1}} \tag{36}$$

$$k_2 = \frac{\sigma_{n,2}}{\sigma_{p,2}} \tag{37}$$

And

$$n_{1,1} = N_C exp\left(\frac{E_C - E_{T1}}{kT}\right) \tag{38}$$

$$p_{1,1} = N_V exp\left(\frac{E_C - E_G - E_{T1}}{kT}\right) \tag{39}$$

$$n_{1,2} = N_C exp\left(\frac{E_C - E_{T2}}{kT}\right) \tag{40}$$

$$p_{1,2} = N_V exp\left(\frac{E_C - E_G - E_{T2}}{kT}\right) \tag{41}$$

Sah-Shockley-Evans-Landsberg Statistics:
This statistics is based on [9,13]:

$$\tau_{SS} = \frac{1}{\frac{1}{\tau_1} + \frac{1}{\tau_2}} \tag{42}$$

With

$$\tau_1 = \frac{\tau_{p0,1}(n_0 + n_{1,1} + \Delta n) + \tau_{n0,1}(p_0 + p_{1,1} + \Delta n)}{n_0 + p_0 + \Delta n} \tag{43}$$

$$\tau_2 = \frac{\tau_{p0,2}(n_0 + n_{1,2} + \Delta n) + \tau_{n0,2}(p_0 + p_{1,2} + \Delta n)}{n_0 + p_0 + \Delta n} \tag{44}$$

where n_0 is the equilibrium electron density, p_0 is the equilibrium hole density and Δn is the excess carrier concentration.

And

$$\tau_{n0,1} = \frac{1}{N_2(\sigma_{n,1} + T_{1,1} \times n + T_{2,1} \times p)v_{th}} \tag{45}$$

$$\tau_{p0,1} = \frac{1}{N_2(\sigma_{p,1} + T_{3,1} \times n + T_{4,1} \times p)v_{th}} \tag{46}$$

$$\tau_{n0,2} = \frac{1}{N_2(\sigma_{n,2} + T_{1,2} \times n + T_{2,2} \times p)v_{th}} \tag{47}$$

$$\tau_{p0,2} = \frac{1}{N_2(\sigma_{p,2} + T_{3,2} \times n + T_{4,2} \times p)v_{th}} \tag{48}$$

And

$$N_1 = N_s + N_{s+1} \tag{49}$$

$$N_2 = N_{s+1} + N_{s+2} \tag{50}$$

And

$$N_{s+1} = \frac{N_t}{\alpha_1 + 1 + \frac{1}{\alpha_2}} \tag{51}$$

$$N_s = \alpha_1 N_{s+1} \tag{52}$$

$$N_{s+2} = \frac{N_{s+1}}{\alpha_2} \tag{53}$$

And

$$\alpha_1 = \frac{k_1 + n_{1,1} + p}{k_1 \times n + p_{1,1}} \tag{54}$$

$$\alpha_2 = \frac{k_2 + n_{1,2} + p}{k_2 \times n + p_{1,2}} \tag{55}$$

And

$$k_1 = \frac{\sigma_{n,1} + T_{1,1} \times n + T_{2,1} \times p}{\sigma_{p,1} + T_{3,1} \times n + T_{4,1} \times p} \tag{56}$$

$$k_2 = \frac{\sigma_{n,2} + T_{1,2} \times n + T_{2,2} \times p}{\sigma_{p,2} + T_{3,2} \times n + T_{4,2} \times p} \tag{57}$$

And

$$n_{1,1} = N_C exp\left(\frac{E_C - E_{T1}}{kT}\right) \tag{58}$$

$$p_{1,1} = N_V exp\left(\frac{E_C - E_G - E_{T1}}{kT}\right) \tag{59}$$

$$n_{1,2} = N_C exp\left(\frac{E_C - E_{T2}}{kT}\right) \tag{60}$$

$$p_{1,2} = N_V exp\left(\frac{E_C - E_G - E_{T2}}{kT}\right) \tag{61}$$

Reduced-Sah-Shockley-Evans-Landsberg Statistics:
This statistics is based on [9,13]:

$$\tau_{SS} = \frac{1}{\frac{1}{\tau_1} + \frac{1}{\tau_2}} \tag{62}$$

With

$$\tau_1 = \frac{\tau_{p0,1}(n_0 + n_{1,1} + \Delta n) + \tau_{n0,1}(p_0 + p_{1,1} + \Delta n)}{n_0 + p_0 + \Delta n} \tag{63}$$

$$\tau_2 = \frac{\tau_{p0,2}(n_0 + n_{1,2} + \Delta n) + \tau_{n0,2}(p_0 + p_{1,2} + \Delta n)}{n_0 + p_0 + \Delta n} \tag{64}$$

where n_0 is the equilibrium electron density, p_0 is the equilibrium hole density and Δn is the excess carrier concentration.

And

$$\tau_{n0,1} = \frac{1}{N_2 \sigma_{n,1} v_{th}} \tag{65}$$

$$\tau_{p0,1} = \frac{1}{N_2 \sigma_{p,1} v_{th}} \tag{66}$$

$$\tau_{n0,2} = \frac{1}{N_2 \sigma_{n,2} v_{th}} \tag{67}$$

$$\tau_{p0,2} = \frac{1}{N_2 T_{3,2} \times n v_{th}} \tag{68}$$

And

$$N_1 = N_s + N_{s+1} \tag{69}$$

$$N_2 = N_{s+1} + N_{s+2} \tag{70}$$

And

$$N_{s+1} = \frac{N_t}{\alpha_1 + 1 + \frac{1}{\alpha_2}} \tag{71}$$

$$N_s = \alpha_1 N_{s+1} \tag{72}$$

$$N_{s+2} = \frac{N_{s+1}}{\alpha_2} \tag{73}$$

And

$$\alpha_1 = \frac{k_1 + n_{1,1} + p}{k_1 \times n + p_{1,1}} \tag{74}$$

$$\alpha_2 = \frac{k_2 + n_{1,2} + p}{k_2 \times n + p_{1,2}} \tag{75}$$

And

$$k_1 = \frac{\sigma_{n,1} + T_{1,1} \times n + T_{2,1} \times p}{\sigma_{p,1} + T_{3,1} \times n + T_{4,1} \times p} \tag{76}$$

$$k_2 = \frac{\sigma_{n,2} + T_{1,2} \times n + T_{2,2} \times p}{\sigma_{p,2} + T_{3,2} \times n + T_{4,2} \times p} \tag{77}$$

And

$$n_{1,1} = N_C exp\left(\frac{E_C - E_{T1}}{kT}\right) \tag{78}$$

$$p_{1,1} = N_V exp\left(\frac{E_C - E_G - E_{T1}}{kT}\right) \tag{79}$$

$$n_{1,2} = N_C exp\left(\frac{E_C - E_{T2}}{kT}\right) \tag{80}$$

$$p_{1,2} = N_V exp\left(\frac{E_C - E_G - E_{T2}}{kT}\right) \tag{81}$$

Appendix E. Derivation of the Corrected Effective Density (CED)

Using SRH statistics:

$$\tau_{SRH} = \frac{\tau_{p0}(n_0 + n_1 + \Delta n) + \tau_{n0}(p_0 + p_1 + \Delta n)}{n_0 + p_0 + \Delta n} \tag{82}$$

where n_0 is the equilibrium electron density, p_0 is the equilibrium hole density and Δn is the excess carrier concentration.

Or

$$\tau_{SRH} = \frac{k(n_0 + n_1 + \Delta n) + p_0 + p_1 + \Delta n}{N\sigma_n v_{th,e}(n_0 + p_0 + \Delta n)} \tag{83}$$

With

$$k = \frac{\sigma_n v_{th,n}}{\sigma_p v_{th,p}} \tag{84}$$

The defect density is thus:

$$N_t^* = N\sigma_n v_{th,n} \frac{(n_0 + p_0 + \Delta n)}{k(n_0 + n_1 + \Delta n) + p_0 + p_1 + \Delta n} \tag{25b}$$

If we ignore n1 $\approx$ 0 as the shallow level is near the valence band, we obtain:

$$N_t^* = N\sigma_n v_{th,n} \frac{(n_0 + p_0 + \Delta n)}{k(n_0 + \Delta n) + p_0 + p_1 + \Delta n} \tag{26b}$$

In p-type silicon, $n_0 \ll p_0$ and measuring the lifetime at $\Delta n = \gamma\ p_0$:

$$N_t^* = N\sigma_n v_{th,n} \frac{1 + \gamma}{\gamma k + 1 + \gamma + \frac{p_1}{p_0}} \tag{27b}$$

Similarly in n-type silicon, $n_0 \ll p_0$ and measuring the lifetime at $\Delta n = \gamma\ n_0$:

$$N_t^* = N\sigma_n v_{th,n} \frac{1 + \gamma}{(1 + \gamma)k + \gamma + \frac{p_1}{n_0}} \tag{28b}$$

In p-type, using $\gamma = 0.1$ that is measuring the lifetime at $\Delta n = 0.1\ p_0$:

$$N_t^* = N\sigma_n v_{th,n} \frac{1.1}{0.1k + 1.1 + \frac{p_1}{p_0}} \tag{29b}$$

In n-type using $\gamma = 0.1$ that is measuring the lifetime at $\Delta p = 0.1\ n_0$:

$$N_t^* = N\sigma_n v_{th,n} \frac{1.1}{1.1k + 0.1 + \frac{p_1}{n_0}} \tag{30b}$$

If p_1 and k are known, the impact of shallow levels on the effective defect density can be corrected as follows in p-type silicon:

$$N_t^{**} = N_t^* \frac{0.1k + 0.1 + \frac{p_1}{p_0}}{1.1} \tag{31b}$$

Similarly in n-type silicon:

$$N_t^{**} = N_t^{*} \frac{1.1k + 0.1 + \frac{p_1}{n_0}}{1.1} \quad (32b)$$

Table of Symbols

E_C	conduction band
E_G	bandgap energy
E_T	defect energy level
E_{T1}	energy level of level 1
E_{T2}	energy level of level 2
E_V	valence band
k	capture cross section ratio
k_1	capture cross section ratio of level 1
k_2	capture cross section ratio of level 2
n_0	free electron concentration
n_1	electron density when the Fermi level equates the defect energy level
$n_{1,1}$	electron density when the Fermi level equates the defect energy level 1
$n_{1,2}$	electron density when the Fermi level equates the defect energy level 2
N_S	density of defect in charge state S
N_{S+1}	density of defect in charge state S+1
N_{S+2}	density of defect in charge state S+2
N_t	defect density
N_t^*	effective defect density
N_t^{**}	corrected defect density
p_0	free hole concentration
p_1	hole density when the Fermi level equates the defect energy level
$p_{1,1}$	hole density when the Fermi level equates the defect energy level 1
$p_{1,2}$	hole density when the Fermi level equates the defect energy level 2
T_1	electron capture coefficient when energy is released through a hot electron
T_2	electron capture coefficient when energy is released through a hot hole
T_3	hole capture coefficient when energy is released through a hot electron
T_4	hole capture coefficient when energy is released through a hot hole
$v_{th,n}$	electron thermal velocity
$v_{th,p}$	hole thermal velocity
α_1	occupation fraction of level 1
α_2	occupation fraction of level 2
Δn	excess carrier density
σ_n	electron capture cross section
σ_p	hole capture cross section
τ	effective carrier lifetime
τ_1	lifetime component from level 1
τ_2	lifetime component from level 2
$\tau(t)$	effective carrier lifetime at time t
$\tau(0)$	effective carrier lifetime at time 0
τ_{n0}	electron lifetime
$\tau_{n0,1}$	electron lifetime for level 1
$\tau_{n0,2}$	electron lifetime for level 2
τ_{p0}	hole lifetime
$\tau_{p0,1}$	hole lifetime for level 1
$\tau_{p0,2}$	hole lifetime for level 2
τ_{EL}	Evans-Landsberg component of the effective lifetime
τ_{RSSEL}	Reduced Sah-Shockley-Evans-Landsberg component of the effective lifetime
τ_{SRH}	Shockley-Read-Hall component of the effective lifetime
τ_{SS}	Sah-Shockley component of the effective lifetime
τ_{SSEL}	Sah-Shockley-Evans-Landsberg component of the effective lifetime

References

[1] T. Niewelt, J. Schön, W. Warta, S.W. Glunz, M.C. Schubert, Degradation of crystalline silicon due to boron–oxygen defects, IEEE J. Photovoltaics 7 (1) (Jan. 2017) 383–398, https://doi.org/10.1109/JPHOTOV.2016.2614119.

[2] M.K. Juhl, et al., An open source based repository for defects in silicon, in: 2018 IEEE 7th World Conference on Photovoltaic Energy Conversion (WCPEC) (A Joint Conference of 45th IEEE PVSC, 28th PVSEC 34th EU PVSEC), 2018, https://doi.org/10.1109/PVSC.2018.8547621, 0328–0332.

[3] K. Bothe, J. Schmidt, Electronically activated boron-oxygen-related recombination centers in crystalline silicon, J. Appl. Phys. 99 (1) (Jan. 2006), 013701, https://doi.org/10.1063/1.2140584.

[4] M. Vaqueiro-Contreras, et al., Identification of the mechanism responsible for the boron oxygen light induced degradation in silicon photovoltaic cells, J. Appl. Phys. 125 (18) (May 2019) 185704, https://doi.org/10.1063/1.5091759.

[5] S.W. Glunz, S. Rein, W. Warta, J. Knobloch, W. Wettling, Degradation of carrier lifetime in Cz silicon solar cells, Sol. Energy Mater. Sol. Cell. 65 (1) (Jan. 2001) 219–229, https://doi.org/10.1016/S0927-0248(00)00098-2.

[6] M. Forster, "Compensation Engineering for Silicon Solar Cells.".

[7] A. Herguth, On the lifetime-equivalent defect density: properties, application, and pitfalls, IEEE J. Photovoltaics (2019) 1–13, https://doi.org/10.1109/JPHOTOV.2019.2922470.
[8] F.E. Rougieux, C. Sun, D. Macdonald, Determining the charge states and capture mechanisms of defects in silicon through accurate recombination analyses: a review, Sol. Energy Mater. Sol. Cell. 187 (Dec. 2018) 263–272, https://doi.org/10.1016/j.solmat.2018.07.029.
[9] C.-T. Sah, W. Shockley, Electron-hole recombination statistics in semiconductors through flaws with many charge conditions, Phys. Rev. 109 (4) (Feb. 1958) 1103–1115, https://doi.org/10.1103/PhysRev.109.1103.
[10] A. Hangleiter, Nonradiative recombination via deep impurity levels in semiconductors: the excitonic Auger mechanism, Phys. Rev. B 37 (5) (Feb. 1988) 2594–2604, https://doi.org/10.1103/PhysRevB.37.2594.
[11] A. Hangleiter, Nonradiative recombination via deep impurity levels in silicon: Experiment, Phys. Rev. B 35 (17) (Jun. 1987) 9149–9161, https://doi.org/10.1103/PhysRevB.35.9149.
[12] J. Szmytkowski, A simple model of the trap-assisted recombination with the excitonic Auger mechanism, Eur. Phys. J. Plus 135 (1) (Jan. 2020) 37, https://doi.org/10.1140/epjp/s13360-019-00058-3.
[13] D.A. Evans, P.T. Landsberg, Recombination statistics for auger effects with applications to p-n junctions, Solid State Electron. 6 (2) (Mar. 1963) 169–181, https://doi.org/10.1016/0038-1101(63)90012-1.
[14] K. Levenberg, A method for the solution of certain non-linear problems in least squares, Q. Appl. Math. 2 (2) (1944) 164–168, https://doi.org/10.1090/qam/10666.
[15] T. Niewelt, S. Mägdefessel, M.C. Schubert, Fast in-situ photoluminescence analysis for a recombination parameterization of the fast BO defect component in silicon, J. Appl. Phys. 120 (8) (Aug. 2016), 085705, https://doi.org/10.1063/1.4961423.
[16] T. Niewelt, J. Schön, J. Broisch, W. Warta, M. Schubert, Electrical characterization of the slow boron oxygen defect component in Czochralski silicon, Phys. Status Solidi Rapid Res. Lett. 9 (12) (Dec. 2015) 692–696, https://doi.org/10.1002/pssr.201510357.
[17] J. Schön, T. Niewelt, J. Broisch, W. Warta, M.C. Schubert, Characterization and modelling of the boron-oxygen defect activation in compensated n-type silicon, J. Appl. Phys. 118 (24) (Dec. 2015) 245702, https://doi.org/10.1063/1.4938569.
[18] B. Hallam, et al., Recent insights into boron-oxygen related degradation: evidence of a single defect, Sol. Energy Mater. Sol. Cell. 173 (Dec. 2017) 25–32, https://doi.org/10.1016/j.solmat.2017.06.038.
[19] L. Scheffler, Vl Kolkovsky, J. Weber, Electrical levels in nickel doped silicon, J. Appl. Phys. 116 (17) (Nov. 2014) 173704, https://doi.org/10.1063/1.4901003.
[20] E. Schibli, A.G. Milnes, Lifetime and capture cross-section studies of deep impurities in silicon, Mater. Sci. Eng. 2 (5) (Jan. 1968) 229–241, https://doi.org/10.1016/0025-5416(68)90036-0.
[21] P.W. Anderson, Model for the electronic structure of amorphous semiconductors, Phys. Rev. Lett. 34 (15) (Apr. 1975) 953–955, https://doi.org/10.1103/PhysRevLett.34.953.
[22] N.A. Modine, A.M. Armstrong, M.H. Crawford, W.W. Chow, Highly nonlinear defect-induced carrier recombination rates in semiconductors, J. Appl. Phys. 114 (14) (Oct. 2013) 144502, https://doi.org/10.1063/1.4824065.
[23] V.V. Voronkov, R. Falster, K. Bothe, B. Lim, J. Schmidt, Lifetime-degrading boron-oxygen centres in p-type and n-type compensated silicon, J. Appl. Phys. 110 (6) (Sep. 2011), 063515, https://doi.org/10.1063/1.3609069.
[24] J. Schmidt, A. Cuevas, Electronic properties of light-induced recombination centers in boron-doped Czochralski silicon, J. Appl. Phys. 86 (6) (Sep. 1999) 3175–3180, https://doi.org/10.1063/1.371186.
[25] S. Rein, S.W. Glunz, Electronic properties of the metastable defect in boron-doped Czochralski silicon: unambiguous determination by advanced lifetime spectroscopy, Appl. Phys. Lett. 82 (7) (Feb. 2003) 1054–1056, https://doi.org/10.1063/1.1544431.
[26] D.J. Robbins, Auger recombination at the B centre in gallium arsenide, J. Phys. C Solid State Phys. 13 (36) (Dec. 1980) L1073–L1078, https://doi.org/10.1088/0022-3719/13/36/006.
[27] W. Shockley, W.T. Read, Statistics of the recombinations of holes and electrons, Phys. Rev. 87 (5) (Sep. 1952) 835–842, https://doi.org/10.1103/PhysRev.87.835.
[28] R.N. Hall, Electron-hole recombination in germanium, Phys. Rev. 87 (2) (Jul. 1952), https://doi.org/10.1103/PhysRev.87.387, 387–387.